



## Resonant transport of bosonic carriers through a quantum device

P. S. Muraev <sup>1,2</sup>, D. N. Maksimov,<sup>1,3</sup> and A. R. Kolovsky <sup>1,2</sup>

<sup>1</sup>*Kirensky Institute of Physics, Federal Research Center KSC SB RAS, 660036 Krasnoyarsk, Russia*

<sup>2</sup>*School of Engineering Physics and Radio Electronics, Siberian Federal University, 660041 Krasnoyarsk, Russia*

<sup>3</sup>*IRC SQC, Siberian Federal University, 660041 Krasnoyarsk, Russia*



(Received 13 October 2021; accepted 21 December 2021; published 11 January 2022)

We analyze the current of Bose particles across a tight-binding chain connected at both ends to the particles' reservoirs. Unlike the standard open Bose-Hubbard model, where the presence of reservoirs is taken into account by the Lindbladians acting on the first and last sites of the chain, we use semimicroscopic models for the reservoirs. This allows us to address the case of arbitrary reservoir temperature. In particular, we discuss the phenomenon of the resonant transmission for nearly condensed bosons, where the current across the chain is significantly enhanced for certain values of the gate voltage.

DOI: [10.1103/PhysRevA.105.013307](https://doi.org/10.1103/PhysRevA.105.013307)

### I. INTRODUCTION

Recently, we have witnessed an increase of interest in the open (dissipative) Bose-Hubbard (BH) system, which has become the paradigm for quantum transport with Bose particles [1–11]. Experimentally, there are two main platforms for realizing the open BH model: superconducting circuits, namely, a chain of coupled transmon qubits [3,6,9,11], and cold Bose atoms in optical lattices [1,7,8]. To study quantum transport in the former system, photons are injected into the first transmon of the chain by using a microwave generator and the signal is read from the last transmon in the chain. In the latter system one measures the atomic current across the lattice connecting two atomic reservoirs with different chemical potentials, in the spirit of the laboratory experiment [12] conducted with Fermi atoms. The unique feature of the bosonic system, however, is that with an increase of the carriers' density it shows a transition from the quantum to the classical regime where the BH chain can be viewed as a system of coupled classical oscillators [3,13]. This quantum-to-classical transition for identical particles motivates further study of transport phenomena with bosonic carriers.

In our previous works [10,13] we analyzed the current of Bose particles within the framework of the standard open BH model where the effect of reservoirs is taken into account by introducing the gain and loss Lindblad operators acting on the first and last sites of the chain. In the classical approach this corresponds to the situation where the first and last oscillators are subject to friction and are excited by white noise whose intensity is determined by the mean particle density of the respective reservoirs [13]. Unfortunately, the standard open BH model implies the Markov approximation, which is not justified for low-temperature reservoirs with nearly condensed Bose particles. In the present work we overcome this problem by introducing a non-Markovian open BH model, which is the bosonic analog of the non-Markovian open Fermi-Hubbard model discussed in Ref. [14]. It is shown below that in the pseudoclassical approach the proposed model utilizes, instead

of white noise, a narrowband noise with a well-defined mean frequency. This brings us closer to the experiment [11] and simultaneously to the situation one encounters in solid-state physics for fermions with well-defined Fermi energy. In particular, similar to the fermionic case, we can address the phenomenon of the resonant transmission [15].

### II. NON-MARKOVIAN OPEN BOSE-HUBBARD MODEL

Since we are interested in the non-Markovian case, a microscopic model for the particle reservoirs is required (see Fig. 1). Following Ref. [14], we use as the reservoirs the tight-binding rings of size  $M$  each, where eventually  $M \rightarrow \infty$ . These rings are attached to both ends of the BH chain of length  $L$ . Bosons can hop between the sites of the chain and the sites of the rings with the rates  $J_s$  and  $J_r$ , where  $J_s \sim J_r$ , while the hopping between the chain and the rings is controlled by the coupling constant  $\epsilon \ll J_s, J_r$ . If the chemical potentials or temperatures of the left and right rings are different, we have a directed current across the chain.

#### A. Quantum Hamiltonians and the governing equation

The system dynamics is governed by the master equation for the total density matrix

$$\frac{\partial \hat{\mathcal{R}}}{\partial t} = -i[\hat{\mathcal{H}}, \hat{\mathcal{R}}] + \sum_{j=L,R} [\hat{\mathcal{L}}_g^{(j)}(\hat{\mathcal{R}}) + \hat{\mathcal{L}}_d^{(j)}(\hat{\mathcal{R}})], \quad (1)$$

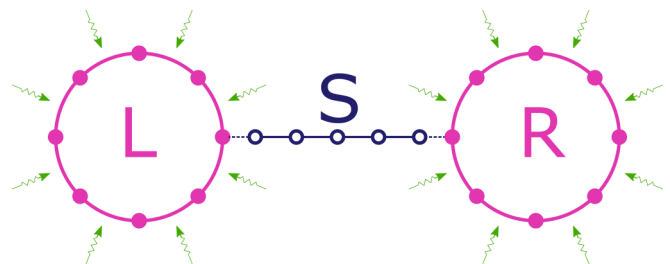


FIG. 1. Schematic presentation of the model.

where the Hamiltonian  $\hat{\mathcal{H}}$  has the form

$$\hat{\mathcal{H}} = \hat{\mathcal{H}}_s + \sum_{j=L,R} \hat{\mathcal{H}}_r^{(j)} + \sum_{j=L,R} \hat{\mathcal{H}}_e^{(j)}. \quad (2)$$

For the chain Hamiltonian  $\hat{\mathcal{H}}_s$  we have

$$\hat{\mathcal{H}}_s = \delta \sum_{\ell=1}^L \hat{n}_\ell - \frac{J_s}{2} \left( \sum_{\ell=1}^{L-1} \hat{a}_{\ell+1}^\dagger \hat{a}_\ell + \text{H.c.} \right) + \frac{U}{2} \sum_{\ell=1}^L \hat{n}_\ell (\hat{n}_\ell - 1), \quad (3)$$

with  $\hat{a}_\ell^\dagger$  and  $\hat{a}_\ell$  the bosonic creation and annihilation operators, respectively, at the  $\ell$ th site. For future purposes we also included in the chain Hamiltonian the on-site energy (gate voltage)  $\delta$  and the interparticle interaction whose strength is characterized by the microscopic interaction constant  $U$ . The ring Hamiltonians  $\hat{\mathcal{H}}_r$  and the coupling Hamiltonians  $\hat{\mathcal{H}}_e$  are indexed by the superscript  $j = L, R$  specifying the ring and we write the ring Hamiltonians in terms of bosonic operators acting in the Fock space of the Bloch states,

$$\hat{\mathcal{H}}_r = \sum_{k=1}^M E_k \hat{b}_k^\dagger \hat{b}_k, \quad E_k = -J_r \cos \left( \frac{2\pi k}{M} \right). \quad (4)$$

Here and below we drop the superscript  $j$  assuming that the rings are identical. The coupling Hamiltonian is given by

$$\hat{\mathcal{H}}_e = -\frac{\epsilon}{2\sqrt{M}} \hat{a}_\ell^\dagger \sum_{k=1}^M \hat{b}_k + \text{H.c.}, \quad (5)$$

where  $\ell = 1$  for  $j = L$  and  $\ell = L$  for  $j = R$ . For the sake of simplicity, we set in what follows  $J_s = J_r \equiv J$ , which in turn is set to unity. Thus all energy constants are measured in units of  $J$ . Also, if not stated otherwise,  $\delta = 0$  and  $U = 0$ .

To prescribe thermodynamic properties to the reservoirs, we introduce the particle drain

$$\hat{\mathcal{L}}_d(\hat{\mathcal{R}}) = -\frac{\gamma}{2} \sum_{k=1}^M (\bar{n}_k + 1) (\hat{b}_k^\dagger \hat{b}_k \hat{\mathcal{R}} - 2\hat{b}_k \hat{\mathcal{R}} \hat{b}_k^\dagger + \hat{\mathcal{R}} \hat{b}_k^\dagger \hat{b}_k) \quad (6)$$

and the particle gain

$$\hat{\mathcal{L}}_g(\hat{\mathcal{R}}) = -\frac{\gamma}{2} \sum_{k=1}^M \bar{n}_k (\hat{b}_k \hat{b}_k^\dagger \hat{\mathcal{R}} - 2\hat{b}_k^\dagger \hat{\mathcal{R}} \hat{b}_k + \hat{\mathcal{R}} \hat{b}_k \hat{b}_k^\dagger), \quad (7)$$

where

$$\bar{n}_k = \frac{1}{e^{\beta(E_k + \mu)} - 1}. \quad (8)$$

These Lindbladians ensure the occupation of the Bloch states of the isolated ( $\epsilon = 0$ ) ring relaxing to the Bose-Einstein distribution with a given chemical potential  $\mu$  and inverse temperature  $\beta$ . The rate at which this relaxation takes place is determined by the constant  $\gamma$ . In what follows we use as the control parameter the particle density  $\bar{n} = \sum_k \bar{n}_k / M$ , which together with the temperature uniquely determines the chemical potential  $\mu$ . We denote the particle densities in the left and right rings by  $\bar{n}_L$  and  $\bar{n}_R$ , respectively.

Our main object of interest is the single-particle density matrix (SPDM) of bosons in the chain which is defined as

$$\rho_{\ell,m}(t) = \text{Tr}[\hat{a}_\ell^\dagger \hat{a}_m \hat{\mathcal{R}}(t)], \quad 1 \leq \ell, m \leq L. \quad (9)$$

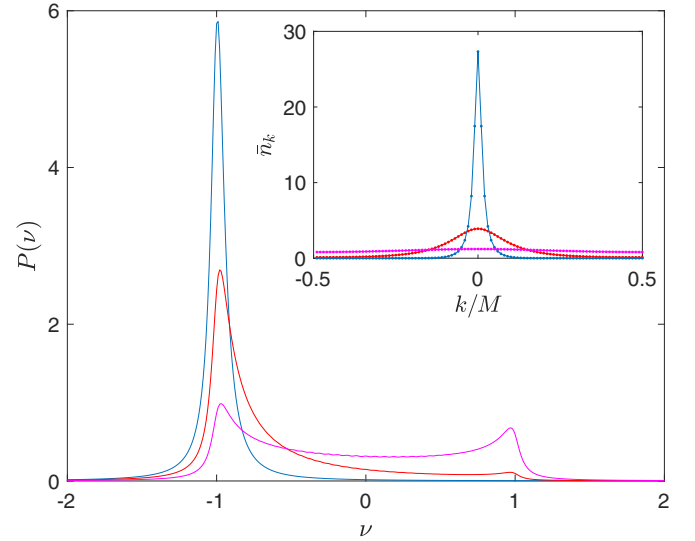


FIG. 2. Spectral density of the stochastic force  $\chi(t)$  for  $\bar{n} = 1$ ,  $\gamma = 0.1$ ,  $M = 100$ , and  $\beta = 0.1, 1, 10$ , from top to bottom, at  $\nu = 0$ . The inset shows the Bose-Einstein distribution for the same temperatures.

Knowing the SPDM, one finds the current in the chain (more precisely, the current density) by using the relation

$$j(t) = \frac{1}{L-1} \text{Tr}[\hat{\rho}(t) \hat{j}], \quad (10)$$

where  $\hat{j}$  is the current operator with the matrix elements  $j_{\ell,m} = J_s(\delta_{\ell,m+1} - \delta_{\ell,m-1})/2i$ . In the case of noninteracting bosons ( $U = 0$ ), the dynamics of the SPDM (9) can be calculated by using at least two different methods. First, one can derive from the original master equation (1) the master equation for the total single-particle density matrix of the size  $(M + L + M) \times (M + L + M)$ , which is then easily solved numerically. The central block of this matrix obviously corresponds to the matrix (9). Below we use this method to calculate Fig. 3 and the dotted line in Fig. 6. The second method employs the pseudoclassical approximation to solve Eq. (1). The main advantage of the pseudoclassical approach is that it can be equally applied to both noninteracting (where it is exact) and interacting bosons. Additionally, it provides deeper insight into the physics of the considered phenomena. We recollect the main points of the pseudoclassical approach in the next section.

## B. Pseudoclassical approach

The pseudoclassical approach replaces the master equation (1) with the Fokker-Planck equation for the classical distribution function  $f$  [13]. Considering for the moment the case of a single ring (generalization to the case of two rings is given at the beginning of Sec. III), the distribution function  $f$  is a function of the time and  $M$  canonical variables  $b_k$  and  $L$  canonical variables  $a_\ell$ . The governing equation reads

$$\frac{\partial f}{\partial t} = \{H, f\} + \sum_k [\mathcal{G}_k(f) + \mathcal{D}_k(f)]. \quad (11)$$

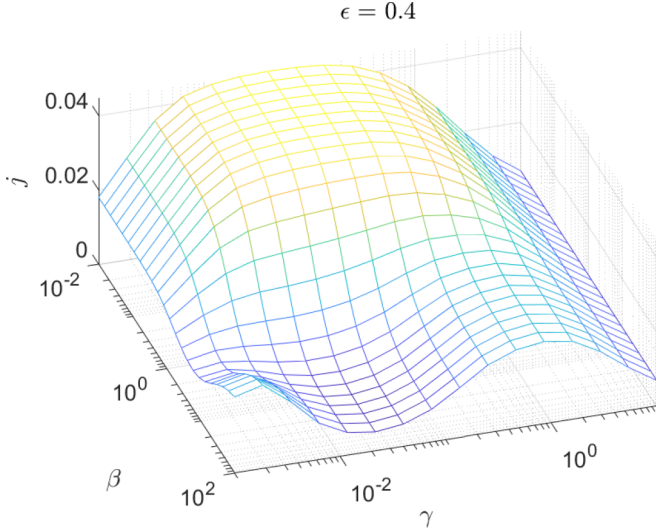


FIG. 3. Stationary current of noninteracting bosons in a chain of length  $L = 5$  connecting two rings with the mean particle densities  $\bar{n}_L = 1$  and  $\bar{n}_R = 0.1$ . The value of the coupling constant  $\epsilon = 0.4$  and the size of the rings  $M = 100$ .

In Eq. (11)  $\{\dots, \dots\}$  denotes the Poisson bracket,  $H$  is the classical Hamiltonian of the system [which is obtained from the quantum Hamiltonian (2) by replacing the creation and annihilation operators with the classical canonical variables], and the last term is the Weyl symbol of the sum of the drain and gain Lindblad operators (6) and (7), respectively. Explicitly we have

$$\mathcal{G}_k(f) = \frac{\gamma}{2} \left( b_k \frac{\partial f}{\partial b_k} + 2f + b_k^* \frac{\partial f}{\partial b_k^*} \right) \quad (12)$$

and

$$\mathcal{D}_k(f) = \gamma \left( \bar{n} + \frac{1}{2} \right) \frac{\partial^2 f}{\partial b_k \partial b_k^*}. \quad (13)$$

It is easy to show that Eq. (12) corresponds to the friction (more precisely, contraction of the phase-space volume) while Eq. (13) describes the diffusion. Thus, the following Langevin equation can be made to correspond to the Fokker-Planck equation (11):

$$idb_k = \left( E_k - i\frac{\gamma}{2} \right) b_k dt + \sqrt{\frac{\gamma \bar{n}_k}{2}} d\xi_k - \frac{\epsilon}{2\sqrt{M}} a_1 dt, \quad (14)$$

$$ida_1 = -\frac{J_s}{2} a_2 dt - \frac{\epsilon}{2} d\chi, \quad \chi(t) = \frac{1}{\sqrt{M}} \sum_k b_k, \quad (15)$$

$$ida_\ell = -\frac{J_s}{2} (a_{\ell-1} + a_{\ell+1}) dt, \quad \ell \neq 1. \quad (16)$$

Here  $\xi_k$  are independent  $\delta$ -correlated random functions and  $\langle d\xi_k(t) d\xi_{k'}(t') \rangle = 2\delta_{k,k'} \delta(t-t') dt$ .

Let us discuss the displayed equations in more detail. For  $\epsilon = 0$ , Eq. (14) is the damped harmonic oscillator subject to white noise. It has the steady-state solution where  $\langle b_k^* b_k \rangle = \bar{n}_k$ . Equations (15) and (16) are the equations of motion for the chain of coupled linear oscillators where the first oscillator is subject to the stochastic force  $\chi(t)$ . We characterize this stochastic force by its spectral density  $P(\nu) = |\chi(\nu)|^2$ , where

$\chi(\nu)$  is the Fourier transform of  $\chi(t)$ . The spectral density  $P(\nu)$  is shown in Fig. 2 for  $\gamma = 0.1$  and three different values of the inverse temperature  $\beta = 0.1, 1, 10$ . It can be seen in Fig. 2 that condensation of bosons in the low-energy Bloch states results in the change of  $\chi(t)$  from a broadband noise to a narrowband noise. We also mention that a further decrease in temperature below  $1/\beta = 0.1$  does not affect the displayed curve because in the limit  $\beta \rightarrow \infty$  its shape is determined by the value of  $\gamma$  but not by the width of the quasimomentum distribution (which tends to a  $\delta$  function). The same is true for temperatures higher than  $1/\beta = 10$  because the quasimomentum distribution is already practically flat for  $\beta = 0.1$ .

### III. STATIONARY CURRENT

We proceed with analysis of the stationary current  $\bar{j} = j(t \rightarrow \infty)$ . To address the transport problem in the framework of the pseudoclassical approach, Eqs. (14)–(16) should be complemented by the equation for the last site of the chain

$$ida_L = -\frac{J_s}{2} a_{L-1} dt - \frac{\epsilon}{2} d\chi_L, \quad \chi_L(t) = \frac{1}{\sqrt{M}} \sum_k b_k^{(R)}, \quad (17)$$

and an equation identical to Eq. (14) for the variables  $b_k^{(R)}$  of the right ring.

#### A. Dependence on system parameters

Figure 3 shows the typical dependence of the stationary current on the relaxation constant  $\gamma$  and the inverse temperature  $\beta$ . As expected, the current vanishes for  $\gamma \rightarrow 0$  where  $\bar{j} \sim \gamma$ . Less expected is that the current also vanishes for  $\gamma \rightarrow \infty$ . Formally, one proves this result by employing the Born and Markov approximations, which are always justified in the above limit and which allow us to eliminate the rings. This reduces the system (1) to the standard open Bose-Hubbard model [10], which is parametrized by the effective relaxation constant

$$\tilde{\gamma} = \epsilon^2 / \gamma. \quad (18)$$

From Eq. (18) we obtain that for  $\gamma \rightarrow \infty$  the current, which is now proportional to  $\tilde{\gamma}$ , decreases as  $\bar{j} \sim 1/\gamma$ . The details of this formal analysis are given in the Appendix.

Next we address the dependence of the stationary current on the temperature. For moderate  $\gamma$  we see in Fig. 3 the pronounced step at  $\beta \sim J$ , where the current drops one order of magnitude (see also Fig. 5). This step is caused by the boson condensation at low temperatures and the pseudoclassical approach provides the necessary details. The top and bottom panels in Fig. 4 show the spectral densities of the stochastic forces  $\chi_1(t)$  and  $\chi_L(t)$ , while the intermediate panels are the spectral densities of the oscillators, i.e., the squared Fourier transform of  $a_\ell(t)$ . The left column in Fig. 4 refers to the case  $\beta = 0.1$ . One can easily identify in the figure the eigenfrequencies  $\omega_i$  and eigenmodes  $X^{(i)}$  of the isolated chain, which are obtained by diagonalizing the chain's single-

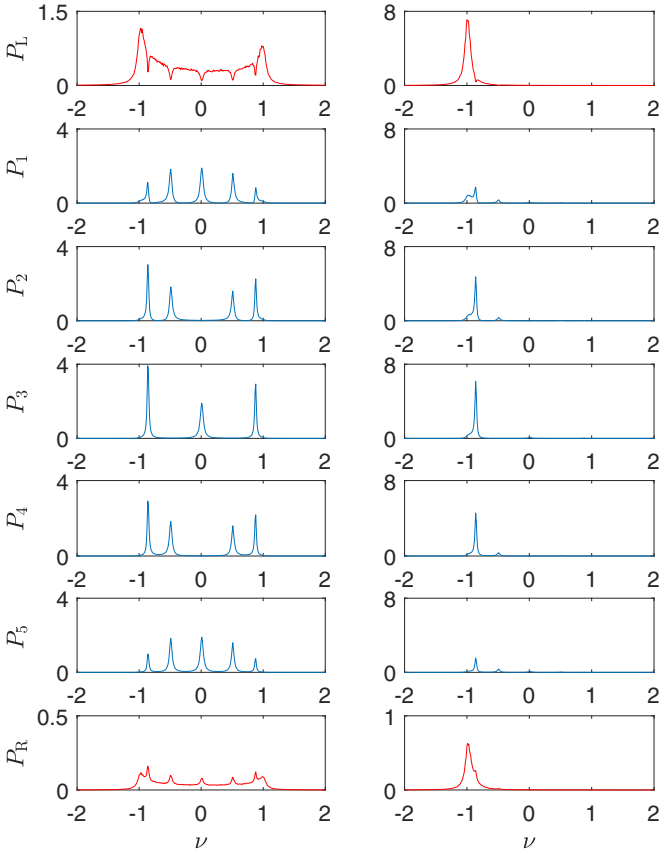


FIG. 4. Spectral densities  $P(\nu)$  of the stochastic forces  $\chi_1(t)$  (top panels) and  $\chi_L(t)$  (bottom panels) for  $\beta = 0.1$  (left column) and  $\beta = 10$  (right column). The intermediate panels show the spectral densities of the local oscillators  $a_\ell(t)$ . The values of the relaxation and coupling constants are  $\gamma = 0.1$  and  $\epsilon = 0.4$ . The particle densities in the left and right reservoirs of size  $M = 100$  are  $\bar{n}_L = 1$  and  $\bar{n}_R = 0.1$ , respectively. Note the different upper limits of the y axes.

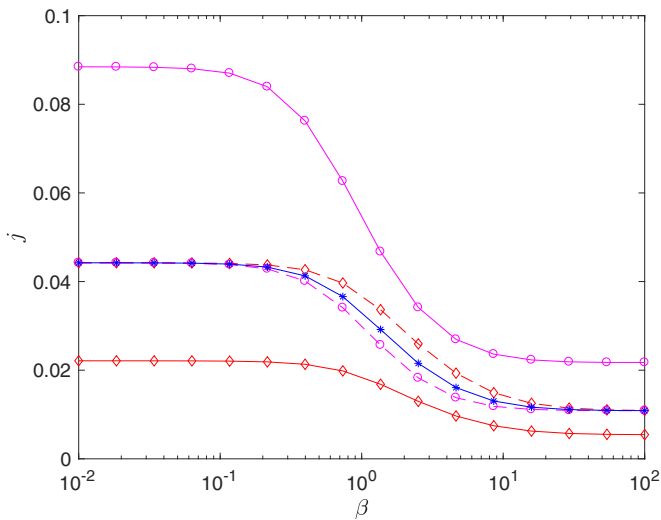


FIG. 5. Stationary current as a function of the inverse temperature for  $\gamma = 0.1$  and  $(\bar{n}_L, \bar{n}_R) = (2, 0.2)$  (top solid line marked by open circles),  $(\bar{n}_L, \bar{n}_R) = (1, 0.1)$  (middle solid line marked by asterisks), and  $(\bar{n}_L, \bar{n}_R) = (0.5, 0.05)$  (bottom solid line marked by diamonds). The dashed lines are the upper and lower curves multiplied by the factors  $1/2$  and  $2$ , respectively.

particle Hamiltonian  $H_s$ ,

$$H_s X^{(i)} = \omega_i X^{(i)}. \quad (19)$$

The positions of the peaks, which are well approximated by a Lorentzian of width  $\sim \epsilon^2$ , coincide with  $\omega_i$ , while the peak heights are proportional to  $|X_\ell^{(i)}|^2$ . Note that for the currently considered  $\beta$  the broadband stochastic force excited all eigenmodes of the chain. The left column in Fig. 4 should be compared with the right column, which refers to the case  $\beta = 10$ . Here the narrowband stochastic force is capable to excite only the lowest mode. Since the group velocity at the bottom of the conduction band tends to zero, we have a much smaller current in the low-temperature limit. In the depicted numerical data we also see the effect of the chain's backaction on the rings. This backaction is smaller for smaller  $\epsilon$ . However, even for the considered  $\epsilon = 0.4$  it can be safely neglected. In other words, in the analytical studies of the problem the spectral density of the stochastic force can be approximated by that shown in Fig. 2 (see also the Appendix).

Finally, let us discuss the dependence of the current on the particle density in the reservoirs. It follows from general arguments that the stationary current across the chain is proportional to the difference  $\bar{n}_L - \bar{n}_R$ . It is also well known that for larger particle density the condensation of bosons occurs at a higher temperature. Thus, the proportional increase of the parameters  $\bar{n}_L$  and  $\bar{n}_R$  will result in the proportional increase of the current. To support this statement Fig. 5 shows the current as a function of the inverse temperature for different particle densities in reservoirs. It can be seen in Fig. 5 that after the linear scaling of the vertical axis (and the proper nonlinear scaling of the temperature axis) all three curves can be put one above the other.

## B. Resonant transmission

The resonant transmission of the fermions is a well-studied phenomenon in solid-state physics [15]. It occurs when the Fermi energy of the reservoirs coincides with an eigenenergy of the mesoscopic device. It is interesting to address the same phenomenon for bosons. Following this goal, we incorporate in all equations the gate voltage  $\delta$ , which determines the onsite energy in the Hamiltonian (1).

Similar to the case of fermions, there are necessary conditions for observing this effect; the crucial condition is that the distance between the energy levels of the mesoscopic device is smaller than the width of the Bose-Einstein distribution in the reservoirs. For the setup considered throughout the paper, these conditions are satisfied, for example, for the parameters used in the right column in Fig. 4. Thus, we may expect a resonancelike behavior of the stationary current under variation of the gate voltage  $\delta$ . Numerical simulations of the system dynamics fully confirm this expectation (see the dotted line in Fig. 6). Note that the positions of the resonant peak are slightly shifted from the expected  $\delta = -(\omega_i + J)$ . This shift increases with an increase of  $\epsilon$  or a decrease of  $\gamma$  and is due to the backaction of the chain on the rings.

Next we study the effect of interparticle interactions on the observed resonant transmission. To do this we use the pseudoclassical approach where the interparticle interactions are characterized by the macroscopic interaction constant  $g =$

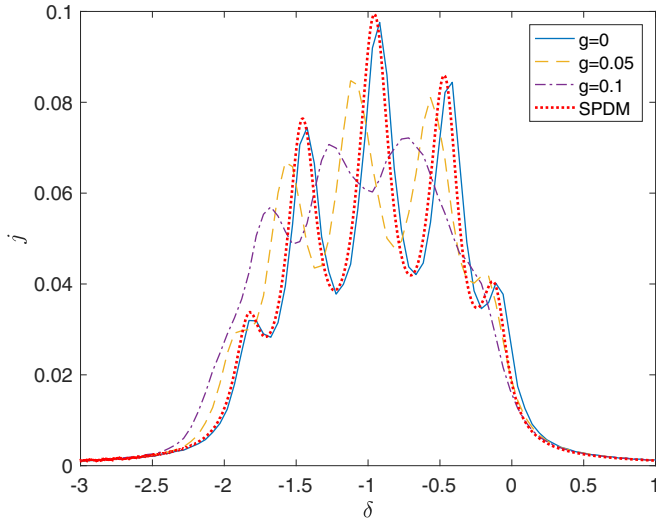


FIG. 6. Stationary current as a function of the gate voltage  $\delta$ . The system parameters are  $\beta = 10$ ,  $\gamma = 0.2$ , and  $\epsilon = 0.4$ . The dotted line is the SPDM solution. The solid, dashed, and dash-dotted lines are the results of the pseudoclassical approach (averaging over 6300 realizations) for  $g = 0, 0.05, 0.1$ , respectively.

$U\bar{n}$ , where, as the parameter  $\bar{n}$ , we choose the mean particle density in the left reservoir. It is known that the pseudoclassical approach is exact for  $g = 0$  and, if  $g \neq 0$ , in the limit  $\bar{n} \rightarrow \infty$  and  $U = g/\bar{n} \rightarrow 0$ . Thus, for a fixed  $\bar{n}$  the method gives correct results only up to some critical  $U$ .

The blue solid line in Fig. 6 corresponds to  $g = 0$  ( $U = 0$ ), where the deviation from the dotted line is due to the finite number of realizations of the stochastic force. This deviation indicates the statistical error for the chosen ensemble with 6300 realizations. The dashed and dash-dotted lines in Fig. 6 refer to  $g \neq 0$ . It can be seen that with an increase of  $g$  the resonant peaks shift to lower values of the gate voltage and simultaneously the resonance pattern fades away.

We find an explanation for the observed effect by analyzing the spectral density  $P_\ell(\nu)$  of the chain oscillators for  $g \neq 0$ . This analysis shows that for the small  $g \leq 0.1$  considered, the stochastic force  $\chi(t)$  mainly excites the collective modes of the system. In more detail, for  $g \neq 0$  and  $\delta \neq 0$  Eq. (16) transforms into

$$i\dot{a}_\ell = (\delta + g|a_\ell|^2)a_\ell - \frac{J_s}{2}(a_{\ell-1} + a_{\ell+1}). \quad (20)$$

Switching to the eigenmode variables (19), Eq. (20) takes the form

$$i\dot{X}^{(i)} = (\delta + \omega_i + gA_i|X^{(i)}|^2)X^{(i)} + g \sum_{j,k \neq i} B_{i,j,k} X^{(i)} X^{(j)} X^{*(k)}, \quad (21)$$

where  $A_i$  and  $B_{i,j,k}$  are constants of the order of unity. For vanishing  $g$  the narrowband stochastic force excites each mode independently. For example, for the parameters of Fig. 6 and  $\delta = -0.5$  this will be the mode  $X^{(2)} = (-1/2, -1/2, 0, 1/2, 1/2)$ , while for  $\delta = -1$  it is  $X^{(3)} = (1/\sqrt{3}, 0, -1/\sqrt{3}, 0, 1/\sqrt{3})$ . If  $g \neq 0$  yet the amplitude of the selected mode is much larger than the amplitudes of the other modes, the mutual influence of the modes [which is described

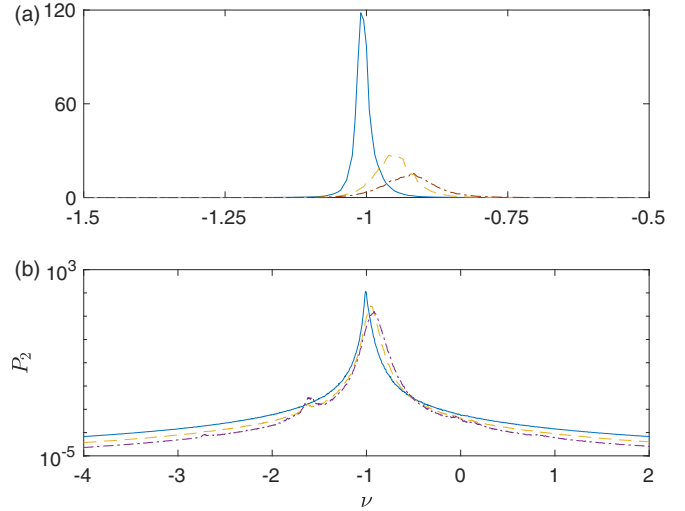


FIG. 7. Spectral density of the eigenmode  $X^{(2)}(t)$  for the parameters of Fig. 6 and  $\delta = -0.5$  in the (a) linear and (b) logarithmic scales. Note the different limits of the horizontal axes.

by the last term in Eq. (21)] can be neglected and we arrive at the problem of the single stochastically driven nonlinear oscillator. Then the main effects are (i) the broadening of the spectral density accompanied by the decrease of its height and (ii) the global shift of the spectral density in the positive direction for positive  $g$  (see Fig. 7). This explains the decrease of the current for the fixed  $\delta = -0.5$  seen in Fig. 6. Note that the shift can be compensated by adjusting  $\delta$  to the new value, which leads to more efficient excitation of the selected mode and, as a consequence, to the appearance of the transmission peak at this value of the detuning.

#### IV. CONCLUSION

We have analyzed the current of Bose particles across a one-dimensional lattice connected at both sides to particle reservoirs. The lattice is modeled by the Bose-Hubbard chain and the reservoirs by bosons in the tight-binding rings, which, if the rings are disconnected from the lattice, relax with the rate  $\gamma$  to the equilibrium state described by the Bose-Einstein distribution. For simplicity, we considered the case of equal reservoir temperatures. Then the stationary current in the lattice is proportional to the difference in the mean particle densities of the reservoirs with the prefactor depending on the temperature  $1/\beta$ , relaxation rate  $\gamma$ , and gate voltage  $\delta$ . The central result of the work is that at low temperature the current as the function of the gate voltage can show pronounced oscillations where it is significantly enhanced for the values of  $\delta$  coinciding with the eigenenergies of the quantum particle in the isolated lattice. Thus, similar to the case of fermionic carriers, we encountered the phenomenon of resonant transmission. We also quantified the role of interparticle interactions in the observed effect and showed that the resonancelike pattern for the current gradually fades out with increasing the interaction constant.

## ACKNOWLEDGMENT

This work was supported by Russian Science Foundation Grant No. N19-12-00167.

## APPENDIX

For noninteracting bosons, the derivation of the master equation for the SPDM (9) is similar to that for fermionic carriers [16]. Of course, one can obtain the master equation in the closed form only under certain assumptions, which are known as the Markov and Born approximations. The former approximation neglects the memory effect in the system dynamics; the latter neglects the backaction of the chain on reservoirs. This means, in particular, that the SPDM of the Bose particles in the reservoirs can be approximated by the thermal density matrix  $\hat{\rho}_r^{(0)}$  determined by the Bose-Einstein distribution (8).

According to Ref. [16], the master equation for the SPDM of the carriers in the chain in the Born approximation reads

$$\frac{\partial \hat{\rho}_s}{\partial t} = -i[\hat{H}_s, \hat{\rho}_s] + \epsilon^2 \sum_{\ell=1,L} (\hat{L}_\ell + \hat{L}_\ell^\dagger), \quad (\text{A1})$$

where  $\hat{H}_s$  is the chain's single-particle Hamiltonian

$$\hat{H}_s = \delta \sum_{\ell=1}^L |\ell\rangle\langle\ell| - \frac{J_s}{2} \sum_{\ell=1}^{L-1} (|\ell+1\rangle\langle\ell| + \text{H.c.}) \quad (\text{A2})$$

and the operators  $\hat{L}_\ell$  have the form

$$\hat{L}_\ell = \frac{|\ell\rangle\langle\ell|}{4} \int_{-t}^0 d\tau e^{(\nu/2)\tau} [\mathcal{J}_F(J_r\tau) \hat{\mathbb{1}}_s - \mathcal{J}_0(J_r\tau) \hat{\rho}_s(\tau+t)] \hat{U}_s(\tau). \quad (\text{A3})$$

In Eq. (A3)  $\mathcal{J}_0$  is the zeroth-order Bessel function of the first kind,  $\hat{\mathbb{1}}_s$  is the identity matrix of the size  $L \times L$ ,  $\hat{U}_s(\tau)$  denotes the evolution operator,  $\hat{U}_s(\tau) = \exp(-i\hat{H}_s\tau)$ , and

$$\mathcal{J}_F(J_r t) = \frac{1}{2\pi} \int_{-\pi}^{\pi} d\kappa \frac{e^{-iJ_r \cos(\kappa)t}}{e^{-\beta[J_r \cos(\kappa)+\mu]} - 1}. \quad (\text{A4})$$

If we now neglect the memory effects, the depicted integro-differential master equation transforms into the Markovian master equation. Formally, this is done by using the general

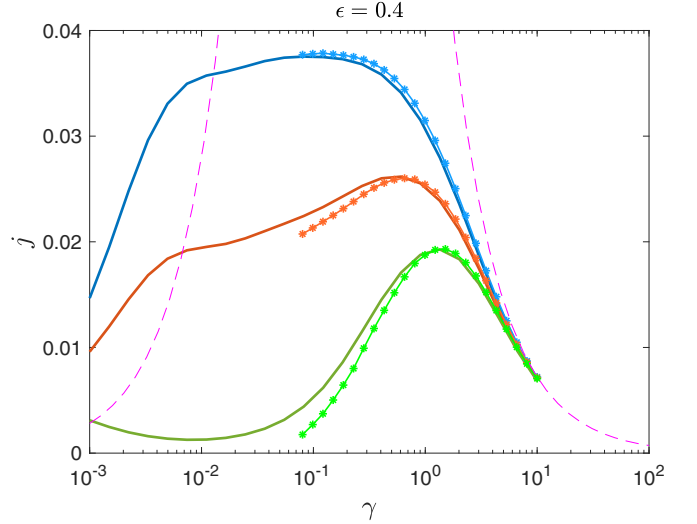


FIG. 8. Comparison of the results based on the Markovian master equation (A6) (dashed line) and the non-Markovian master equation (A1) (solid lines with symbols) with the exact results based on the original model (1) (solid lines). Different solid lines in the figure refer to different inverse temperatures  $\beta = 0.1, 1, 10$ , from top to bottom.

relation for any slowly varying function

$$\int_0^t d\tau e^{(\nu/2)\tau} \mathcal{A}(\tau+t) \approx \frac{2}{\gamma} \mathcal{A}(t), \quad (\text{A5})$$

which becomes exact in the limit  $\gamma \rightarrow \infty$ . This gives

$$\frac{\partial \hat{\rho}_s}{\partial t} = -i[\hat{H}_s, \hat{\rho}_s] - \tilde{\gamma} \sum_{\ell=1,L} \left( \frac{1}{2} \{|\ell\rangle\langle\ell|, \hat{\rho}_s\} - \bar{n}_\ell |\ell\rangle\langle\ell| \right), \quad (\text{A6})$$

where  $\tilde{\gamma} = \epsilon^2/\gamma$ . Equation (A6) is the SPDM master equation of the standard open BH model. It admits the analytical solution with the following result for the stationary current [10]:

$$\bar{j} = J_s \frac{J_s \tilde{\gamma}}{J_s^2 + \tilde{\gamma}^2} \frac{\bar{n}_L - \bar{n}_R}{2}. \quad (\text{A7})$$

It is interesting to discuss the validity of the Born and Markov approximations with respect to the numerical data presented in Fig. 3. The solid lines in Fig. 8 are the sections of Fig. 3 for  $\beta = 0.1$  (high temperature),  $\beta = 1$  (moderate temperature), and  $\beta = 10$  (low temperature). The dashed magenta line is the result obtained on the basis of the Markovian master equation (A6). It can be seen that the Markov approximation is justified only for the large  $\gamma > 5$ . Unlike the Markovian master equation, the non-Markovian master equation (A1) is seen to be valid until  $\gamma \approx 0.1$ . Thus it is particularly capable of describing the phenomenon of resonant transmission considered in Sec. III.

[1] G. Barontini, R. Labouvie, F. Stubenrauch, A. Vogler, V. Guarrera, and H. Ott, Controlling Dynamics of an Open Many-Body Quantum System with Localized Dissipation, *Phys. Rev. Lett.* **110**, 035302 (2013).

[2] A. Ivanov, G. Kordas, A. Komnik, and S. Wimberger, Bosonic transport through a chain of quantum dots, *Eur. Phys. J. B* **86**, 345 (2013).

[3] J. Raftery, D. Sadri, S. Schmidt, H. E. Türeci, and A. A. Houck,

- Observation of a Dissipation-Induced Classical to Quantum Transition, *Phys. Rev. X* **4**, 031043 (2014).
- [4] G. Kordas, D. Witthaut, P. Buonsante, A. Vezzani, R. Burioni, A. I. Karanikas, and S. Wimberger, The dissipative Bose-Hubbard model, *Eur. Phys. J. Spec. Top.* **224**, 2127 (2015).
- [5] G. Kordas, D. Witthaut, and S. Wimberger, Non-equilibrium dynamics in dissipative Bose-Hubbard chains, *Ann. Phys. (Berlin)* **527**, 619 (2015).
- [6] S. Hacothen-Gourgy, V. V. Ramasesh, C. De Grandi, I. Siddiqi, and S. M. Girvin, Cooling and Autonomous Feedback in a Bose-Hubbard Chain with Attractive Interactions, *Phys. Rev. Lett.* **115**, 240501 (2015).
- [7] R. Labouvie, B. Santra, S. Heun, S. Wimberger, and H. Ott, Negative Differential Conductivity in an Interacting Quantum Gas, *Phys. Rev. Lett.* **115**, 050601 (2015).
- [8] R. Labouvie, B. Santra, S. Heun, and H. Ott, Bistability in a Driven-Dissipative Superfluid, *Phys. Rev. Lett.* **116**, 235302 (2016).
- [9] M. Fitzpatrick, N. M. Sundaresan, A. C. Y. Li, J. Koch, and A. A. Houck, Observation of a Dissipative Phase Transition in a One-Dimensional Circuit QED Lattice, *Phys. Rev. X* **7**, 011016 (2017).
- [10] A. R. Kolovsky, Z. Denis, and S. Wimberger, Landauer-Büttiker equation for bosonic carriers, *Phys. Rev. A* **98**, 043623 (2018).
- [11] G. P. Fedorov, S. V. Remizov, D. S. Shapiro, W. V. Pogosov, E. Egorova, I. Tsitsilin, M. Andronik, A. A. Dobronosova, I. A. Rodionov, O. V. Astafiev, and A. V. Ustinov, Photon Transport in a Bose-Hubbard Chain of Superconducting Artificial Atoms, *Phys. Rev. Lett.* **126**, 180503 (2021).
- [12] M. Lebrat, P. Grisins, D. Husmann, S. Häusler, L. Corman, T. Giamarchi, J.-P. Brantut, and T. Esslinger, Band and Correlated Insulators of Cold Fermions in a Mesoscopic Lattice, *Phys. Rev. X* **8**, 011053 (2018).
- [13] A. A. Bychek, P. S. Muraev, D. N. Maksimov, and A. R. Kolovsky, Open Bose-Hubbard chain: Pseudoclassical approach, *Phys. Rev. E* **101**, 012208 (2020).
- [14] A. R. Kolovsky, Open Fermi-Hubbard model: Landauer's versus master equation approaches, *Phys. Rev. B* **102**, 174310 (2020).
- [15] S. Datta, *Electronic Transport in Mesoscopic Systems* (Cambridge University Press, Cambridge, 1995).
- [16] A. R. Kolovsky and D. N. Maksimov, Resonant transmission of fermionic carriers: Comparison between solid-state physics and quantum optics approaches, *Phys. Rev. B* **104**, 115115 (2021).